Letters

Split Impedance Tuning of Multistrand PCB Windings for Constructing Efficient Wireless Power Transfer Module

Junhua Wang, *Member, IEEE*, Xinghong He, Changsong Cai, *Senior Member, IEEE*, Yang Si, and Jing Xiao

***Abstract*—Printed circuit board (PCB) windings offer significant advantages for various applications, including ease of manufacturing, high repeatability, and compact size. These qualities are particularly beneficial in modular wireless power transfer (WPT) systems for uncrewedaerial vehicles, and other mobile devices, which require compact dimensions and consistent parameters. However, a major challenge associated with PCB windings is substantial high-frequency ac resistance. To address this issue, this letter proposes a split impedance tuning method that is free from complex design. It employs capacitors to tune the impedance of each strand, thereby achieving optimal current distribution and reducing resistance. Experimental validation demonstrates that the proposed method reduces the resistance of the tested sample from 0.904 to 0.326 Ω. The 527-W experimental WPT system, utilizing 76-mm-radius PCB windings operating at 300 kHz, achieves 90% efficiency.**

***Index Terms*—AC resistance, Printed circuit board (PCB), split impedance tuning, uncrewedaerial vehicles (UAVs), wireless power transfer (WPT).**

I. Introduction

With the advancement of integration in power electronics, printed circuit boards (PCBs) have become a prominent manufacturing method for coupling windings in wireless power transfer (WPT) systems, particularly for mobile devices, uncrewedaerial vehicles, and other intelligent devices that necessitate a lightweight receiver design [1], [2]. This is attributed to their ease of production, high reliability, and lightweight characteristics [3]. However, the skin effect and proximity effect increase ac resistance significantly at higher operating frequencies, posing challenges for PCB winding applications. Mitigating these effects is crucial for optimizing ac resistance in PCBs.

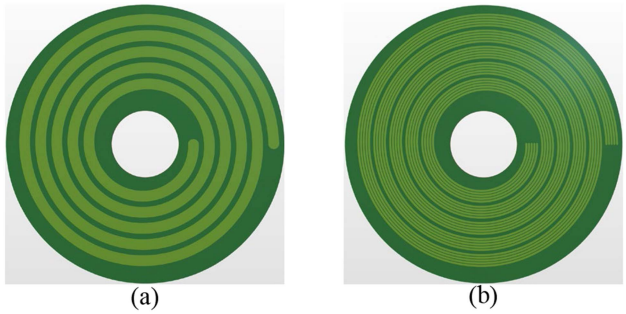

Fig. 1. PCB windings. (a) Single strand. (b) Multistrand.

First, as illustrated in Fig. 1, to mitigate the skin effect, a single-strand PCB winding is commonly divided into multiple strands. However, the reduction in ac resistance is limited due to the proximity effect among the strands. To further minimize the ac resistance, substantial optimization research has been conducted on structural parameters, such as line width, line spacing, and the number of split strands [4]. However, the direct division into parallel strands leads to nonequivalent tracks. To address this issue, a litz structure utilizing the twisting technique is proposed, which can achieve equivalence among strands while also minimizing the total flux linkage between pairs of tracks [5], [6]. To address the issue of inductance reduction resulting from path length differences between the inner and outer strands, a novel structure has been proposed. In this design, wires are systematically rotated from the top layer to the bottom layer, thereby ensuring consistent lengths of the split wires [7].

As the system frequency enters the MHz range, distributed capacitance and dielectric loss become increasingly significant and must be taken into account. To mitigate interwinding capacitance and dielectric loss, a novel resonant structure has been proposed, which separates the two planar windings using air gaps [8]. A design for a PCB resonator winding optimized via the partial element equivalent circuit method has been proposed for implementation in Domino WPT [9]. A multilayer nonuniform

Received 31 March 2025; revised 28 April 2025; accepted 22 May 2025. Date of publication 26 May 2025; date of current version 5 August 2025. This work was supported in part by the National Natural Science Foundation of China under Grant U24A20144, Grant 52207013, in part by the National Key Research and Development Program of China under Grant 2024YFC2417902, and in part by the Hubei Provincial Natural Science Foundation of China under Grant 2024AFB745. *(Corresponding author: Changsong Cai.)*

Junhua Wang, Xinghong He, and Changsong Cai are with the Hubei Key Laboratory of Power Equipment & System Security for Integrated Energy, School of Electrical Engineering and Automation, Wuhan University, Wuhan 430072, China (e-mail: junhuawang@whu.edu.cn; xinghonghe@whu.edu.cn; changsongcai@whu.edu.cn).

Yang Si is with the Qinghai Provincial Key Laboratory of Clean Energy Efficient Utilization, School of Energy and Electrical Engineering, Qinghai University, Xining 810016, China (e-mail: siyang@qhu.edu.cn).

Jing Xiao is with the Southern Power Grid Corporation Wireless Power Transmission Joint Laboratory, Guangxi Power Grid Company, Ltd., Nanning 530000, China (e-mail: xiao_j.sy@gx.csg.cn).

Color versions of one or more figures in this article are available at https://doi.org/10.1109/TPEL.2025.3573853.

Digital Object Identifier 10.1109/TPEL.2025.3573853

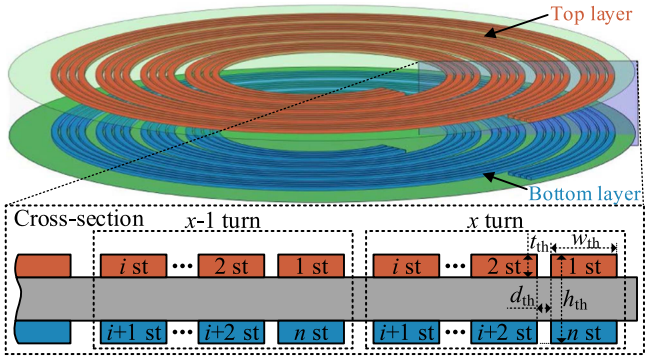

Fig. 2. 3-D and cross-sectional of a double-layer PCB winding.

self-resonant winding designed for high-power, high-frequency wireless electric vehicle charging has been proposed. This design incorporates interlayer capacitors to achieve resonance, thereby enhancing the efficiency and performance of the system [10]. A multimegahertz WPT technology employing integrated PCB self-resonators is introduced, capable of achieving both magnetic coupling wireless power transfer (MC-WPT) and electric-field coupled WPT [11].

In addition to the PCB structure, relevant research has also focused on materials. By employing a substrate with a high dielectric constant in conjunction with a high-precision PCB structure, a thin metamaterial exhibiting negative relative permeability and low loss was fabricated at 6.78 MHz. [12].

As the frequency increases, the resistance of the PCB winding rises due to the skin effect and proximity effect. Consequently, previous research has predominantly focused on optimizing these effects while consistently neglecting the variations in resistance and inductance among individual wire strands. Such variations cause an imbalance in current distribution, which in turn increases the overall equivalent resistance of the winding. To address this issue, this letter proposes a circuit model for multistrand wires, analyzes and derives the optimal current distribution, and introduces split impedance tuning as a method to optimize current distribution and thereby reduce winding loss. The main advantages of proposed method can be summarized as follows.

1) *Simplicity in design:* Without extensive design and simulation, the optimal current distribution among multistrand wires achieved merely through capacitors, significantly reducing the equivalent resistance of the PCB winding.
2) *Broad applicability:* Unlike methods that focus on direct optimization of the winding itself, this approach is not constrained by factors, such as frequency or PCB winding dimensions, and thus can be universally applied to optimize any multistrand PCB windings.

II. Modeling and Analysis of the Split Wire

A. Modeling of Split Wire

Fig. 2 illustrates the cross-section of a multistrand PCB winding. Each wire is composed of n strands arranged in parallel,

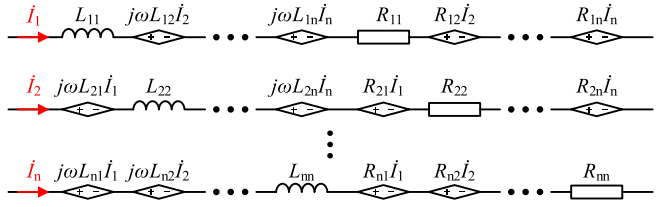

Fig. 3. Equivalent model of multistrand wire.

which can mitigate the skin effect. However, each strand still influences each other, a phenomenon known as the proximity effect.

Fig. 3 is an equivalent model of the multistrand conductor. $\dot{I}i$ represents the currents flowing through the ith strand. L_{ii} and R_{ii} are the self-inductance and resistance of the ith strand, respectively. L_{ij} and R_{ij} ($i \neq j$) represent the mutual inductance and mutual resistance of the ith and jth strands, respectively. The angular frequency of the system, denoted as ω, is related to the operating frequency f by the equation $\omega = 2\pi f$.

The mathematical model for the equivalent resistance and inductor of a multistrand wire can be expressed as follows:

$$\boldsymbol{R}_{\mathbf{mat}} = \begin{bmatrix} R_{11} & R_{12} & \cdots & R_{1n} \\ R_{21} & R_{22} & \cdots & R_{2n} \\ \vdots & \vdots & \ddots & \vdots \\ R_{n1} & R_{n2} & \cdots & R_{nn} \end{bmatrix},$$

$$\boldsymbol{L}_{\mathbf{mat}} = \begin{bmatrix} L_{11} & L_{12} & \cdots & L_{1n} \\ L_{21} & L_{22} & \cdots & L_{2n} \\ \vdots & \vdots & \ddots & \vdots \\ L_{n1} & L_{n2} & \cdots & L_{nn} \end{bmatrix}. \tag{1}$$

The matrix representing the current flowing through each strand can be expressed as follows:

$$\boldsymbol{I}_{\mathbf{mat}} = \begin{bmatrix} \dot{I}_1 & \dot{I}_2 & \cdots & \dot{I}_n \end{bmatrix}^{\mathrm{T}} \tag{2}$$

where the symbol T, located in the upper right corner, signifies the transposition of the matrix. It is worth noting that to distinguish between matrices and complex numbers, matrices will be uniformly represented in bold, while complex numbers will be indicated with a dot above the symbol.

B. Analysis and Optimization of Loss

To facilitate analysis, the column matrix consisting entirely of one with n rows is defined as Λ

$$\boldsymbol{\Lambda} = \begin{bmatrix} 1 & 1 & \cdots & 1 \end{bmatrix}^{\mathrm{T}}. \tag{3}$$

The wire is formed by connecting each strand in parallel at both ends, thus the voltage at both ends of each strand is defined as $\dot{U}_{\mathrm{X}}$. According to Kirchhoff's voltage law, the Kirchhoff's voltage law (KVL) equation is expressed as follows:

$$\dot{U}_{\mathrm{x}}\boldsymbol{\Lambda} = (j\omega\boldsymbol{L}_{\mathbf{mat}} + \boldsymbol{R}_{\mathbf{mat}}) \cdot \boldsymbol{I}_{\mathbf{mat}}. \tag{4}$$

By solving (4), the current matrix can be obtained as follows:

$$\boldsymbol{I}_{\mathbf{mat}} = (j\omega\boldsymbol{L}_{\mathbf{mat}} + \boldsymbol{R}_{\mathbf{mat}})^{-1} \cdot \dot{U}_{\mathrm{x}}\boldsymbol{\Lambda}. \tag{5}$$

Therefore, the winding loss can be expressed as

$$P_{\text{Loss}} = \boldsymbol{I_{mat}}^{\text{T}} \cdot \boldsymbol{R_{mat}} \cdot \boldsymbol{I_{mat}}^{\text{H}} \tag{6}$$

where H, located in the upper right corner, denotes the conjugate operation of the complex numbers. The sum of the currents flowing through each strand can be calculated by

$$\dot{I}_{\text{x}} = \boldsymbol{\Lambda}^{\text{T}} \cdot \boldsymbol{I_{mat}}. \tag{7}$$

The equivalent impedance $\dot{Z}_{\text{x}}$ of the winding can be calculated as follows:

$$\dot{Z}_{\text{x}} = \frac{\dot{U}_{\text{x}}}{\dot{I}_{\text{x}}} = \frac{1}{\boldsymbol{\Lambda}^{\text{T}} \cdot (j\omega \boldsymbol{L_{mat}} + \boldsymbol{R_{mat}})^{-1} \cdot \boldsymbol{\Lambda}}. \tag{8}$$

The equivalent resistance and inductance of the winding can be determined by calculating the real and imaginary components of the impedance

$$\begin{cases} R_{\text{eq}} = \text{Re}\left(\dot{Z}_{\text{x}}\right) \\ L_{\text{eq}} = \frac{\text{Im}\left(\dot{Z}_{\text{x}}\right)}{\omega} \end{cases} \tag{9}$$

where $\text{Re}(*)$ and $\text{Im}(*)$ represent the real and imaginary parts of the complex number, respectively.

The quality factor Q of the winding can be calculated by

$$Q = \frac{\omega L_{\text{eq}}}{R_{\text{eq}}}. \tag{10}$$

To attain the current distribution that minimizes loss, the Lagrange function is formulated by considering (7) as the constraint condition

$$\begin{aligned} \Gamma\left(\boldsymbol{I_{mat}}, \lambda\right) = {} & \boldsymbol{I_{mat}}^{\text{T}} \cdot \boldsymbol{R_{mat}} \cdot \boldsymbol{I_{mat}}^{\text{H}} \\ & + \lambda\left(\dot{I}_{\text{x}} - \dot{I}_1 - \dot{I}_2 \cdots \dot{I}_{\text{n}}\right) \end{aligned} \tag{11}$$

where λ is the Lagrange multiplier. By calculating the partial derivative of the Lagrange function with respect to each variable and setting it to zero, the equation can be obtained as

$$\nabla_{\boldsymbol{I_{mat}}} \Gamma\left(\boldsymbol{I_{mat}}, \lambda\right) = \begin{bmatrix} 0 & 0 & \cdots & 0 \end{bmatrix}^{\text{T}} \tag{12}$$

$$\frac{\partial \Gamma\left(\boldsymbol{I_{mat}}, \lambda\right)}{\partial \lambda} = 0. \tag{13}$$

By resolving (12) and (13), the optimal current matrix can be ascertained as follows:

$$\boldsymbol{I}_{\text{op}} = \frac{\boldsymbol{R_{mat}}^{-1} \cdot \boldsymbol{\Lambda}}{\boldsymbol{\Lambda}^{\text{T}} \cdot \boldsymbol{R_{mat}}^{-1} \cdot \boldsymbol{\Lambda}} \dot{I}_{\text{x}}. \tag{14}$$

III. Design and Analysis of System Parameters

A. Design of the Split Impedance Tuning

Considering the current as a reference (where the imaginary part of the current is zero), the voltage $\boldsymbol{U}_{\text{op}}$ across each strand in the optimal current distribution is

$$\boldsymbol{U}_{\text{op}} = (j\omega \boldsymbol{L_{mat}} + \boldsymbol{R_{mat}}) \cdot \boldsymbol{I}_{\text{op}}. \tag{15}$$

By substituting (14) into (15), it is evident that all real parts of the voltages are equivalent. Fig. 4(a) illustrates the voltage and current diagram of the winding composed of three strands.

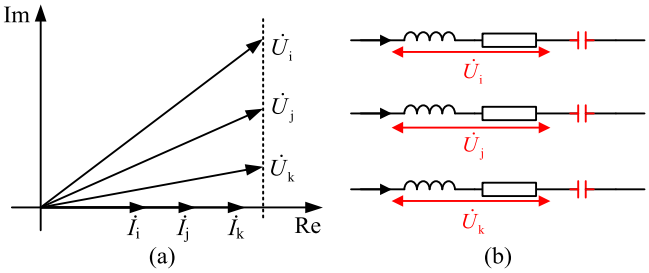

Fig. 4. (a) Schematic diagram of voltage and current vectors. (b) Circuit of split impedance tuning.

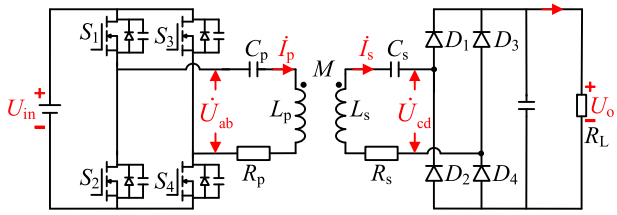

Fig. 5. Circuit structure of the WPT system.

To compensate the voltage discrepancies, a split impedance tuning method is proposed, wherein capacitors are connected in series with each strand to compensate for the reactive voltage, as shown in Fig. 4(b).

By considering the voltage with the smallest imaginary component as the reference point, the voltage differences between each strand and this minimum voltage can be explicitly represented as

$$\boldsymbol{dU} = \omega \boldsymbol{L_{mat}} \cdot \boldsymbol{I}_{\text{OP}} - \min\left(\omega \boldsymbol{L_{mat}} \cdot \boldsymbol{I}_{\text{OP}}\right) \tag{16}$$

where $\min(*)$ denotes the minimum value of the matrix. Thus, the compensation capacitor C_{i} for the ith strand can be calculated by

$$C_i = \frac{\boldsymbol{I}_{\text{OP}}[i]}{\boldsymbol{dU}[i]\,\omega} \tag{17}$$

where $[i]$ represents the ith elements of the matrix. The equivalent resistance and inductance of the winding after split impedance tuning are as follows:

$$\begin{cases} R_{\text{eq}} = \frac{1}{\boldsymbol{\Lambda}^{\text{T}} \cdot \boldsymbol{R_{mat}}^{-1} \cdot \boldsymbol{\Lambda}} \\ L_{\text{eq}} = \frac{\min(\omega \boldsymbol{L_{mat}} \cdot \boldsymbol{I}_{\text{OP}})}{\omega I_{\text{x}}} \end{cases}. \tag{18}$$

B. Design of the WPT System

The circuit structure of the WPT system is illustrated in Fig. 5. The input and output voltages of the system are denoted as U_{in} and U_{o}, respectively, with corresponding equivalent ac voltage represented as $\dot{U}_{\text{ab}}$ and $\dot{U}_{\text{cd}}$. MOSFETs S_1–S_4 and diodes D_1–D_4 constitute the inverter and rectifier, respectively.

C_{p} and C_{s} are resonator capacitors. L_{p} and L_{s} represent the transmitter and receiver, respectively, with the corresponding resistance being R_{p} and R_{s}. The currents flowing through L_{p} and L_{s} are denoted as $\dot{I}_{\text{p}}$ and $\dot{I}_{\text{s}}$. M represents mutual inductance.

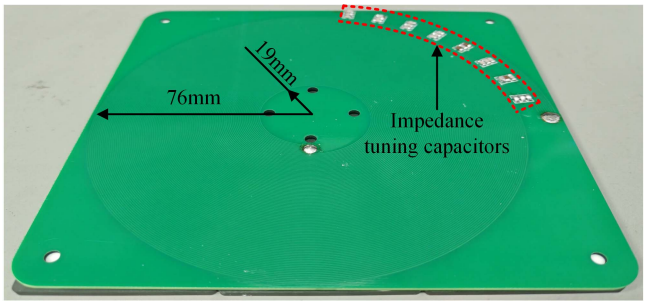

Fig. 6. Experimental test sample of PCB winding.

R_L is the dc load. The circuit components should satisfy

$$\omega = 1/\sqrt{L_p C_s} = 1/\sqrt{L_s C_s}. \tag{19}$$

Assuming the resistance is neglected, the KVL equation for the circuit can be expressed as follows:

$$\begin{bmatrix} 0 & -j\omega M \\ -j\omega M & R_{ac} \end{bmatrix} \begin{bmatrix} \dot{I}_p \\ \dot{I}_s \end{bmatrix} = \begin{bmatrix} \dot{U}_{ab} \\ 0 \end{bmatrix} \tag{20}$$

where R_{ac} represents the ac load, expressed as $R_{ac} = (8/\pi^2)\, R_L$. By solving (20), the output power P_o can be calculated by

$$P_o = \frac{64 U_{in}^2}{\pi^4 \omega^2 M^2} R_L. \tag{21}$$

C. Power Losses Analysis

The system losses are primarily divided into three components: inverter loss P_{Inv}, coupler loss P_{Cou}, and rectifier loss P_{Rec}.

According to Li et al. [13], the P_{Inv} includes the losses generated by four MOSFETs S_1–S_4, which consist of turn-ON loss, turn-OFF loss, reverse recovery loss, and conduction loss. Therefore, P_{Inv} can be expressed as

$$P_{Inv} = 4 U_{in} f_s \left[\frac{e_{ON} + e_{OFF}}{V_R I_R} + \frac{Q_{RR}}{I_{RD}} \right] i_{sw} + 2 {I_p}^2 R_{con} \tag{22}$$

where R_{con} is drain–source ON-state resistance, e_{ON} and e_{OFF} are the turn-ON and turn-OFF loss of MOSFETs under reference voltage V_R and current I_R, respectively. i_{sw} is the switching current of inverter. Q_{RR} and I_{RD} are reverse recovery charge and the reference current of the MOSFETs, respectively.

The coupler loss is composed of transmitter and receiver loss and can be expressed as

$$P_{Cou} = I_p^2 R_p + I_s^2 R_s. \tag{23}$$

The diodes D_1–D_4 form the full-bridge rectifier, with a forward voltage of V_{fs}. Therefore, P_{Rec} can be calculated by

$$P_{Rec} = \frac{4\sqrt{2}}{\pi} I_s V_{Fs}. \tag{24}$$

Therefore, the total loss of the system is the sum of three parts, which can be expressed as

$$P_{Loss} = P_{Inv} + P_{Cou} + P_{Rec}. \tag{25}$$

TABLE I
ELECTRICAL PARAMETERS OF THE PCB WINDING

	Symbol	Value	
		Before impedance tuning	After impedance tuning
Calculation	L_{ab}'	19.5 μH	19.4 μH
	R_{ab}'	0.895 Ω	0.306 Ω
Measurement	L_{ab}	19.9 μH	19.7 μH
	R_{ab}	0.904 Ω	0.326 Ω

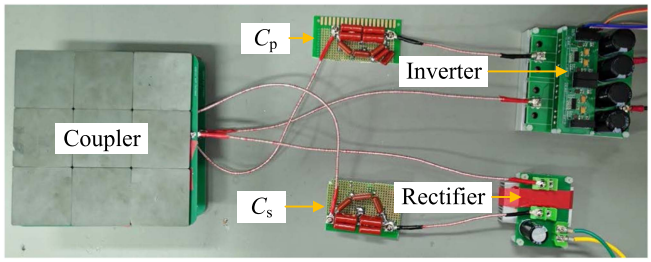

Fig. 7. Experimental platform of the WPT system based on PCB windings.

TABLE II
ELECTRICAL PARAMETERS OF THE WPT SYSTEM

Symbol	Value	Symbol	Value
M	7.2 μH	U_{in}	100 V
L_p	19.7 μH	C_p	14.3 nF
L_s	19.7 μH	C_s	14.3 nF

IV. EXPERIMENTAL VERIFICATION

To verify the theoretical analysis, a tested sample of multi-strand parallel PCB winding, as shown in Fig. 6, was fabricated, with an outer diameter of 76 mm and an inner diameter of 19 mm. The structure is identical to the one shown in Fig. 2, which consists of a double-layer PCB with a thickness (h_{th}) of 1.6 mm. Each layer contains eight strands arranged in parallel spirals, with a total of 12 turns (x). Each strand has a width (w_{th}) of 0.44 mm, a thickness (t_{th}) of 0.07 mm, and a spacing (d_{th}) of 0.16 mm. At a 1-mm spacing beneath the winding, nine ferrite pieces, each measuring 50 mm × 50 mm × 2.5 mm, are arranged. The tuning capacitors utilized in the experiment are multilayer ceramic capacitors with a dielectric material classified as Type I ceramic. They exhibit a temperature coefficient of 0 × (−1) ppm/°C ± 30 ppm/°C (C0G) and have a package size of 0.12 in × 0.6 in (1206).

Table I presents the equivalent inductance and equivalent resistance of the PCB winding, both before and after impedance tuning, as obtained through calculations (L_{ab}', R_{ab}') and measurements (L_{ab}, R_{ab}) under 300 kHz. It should be noted that the calculated values are derived by first measuring the specific values in (1) using the impedance analyzer, and then substituting these values into (9) and (18) for subsequent calculations. The resistance of the winding decreases from 0.904 to 0.326 Ω.

A 527-W experimental platform was established, as illustrated in Fig. 7, based on the circuit structure in Fig. 5.

TABLE III
COMPARISON BETWEEN THE [4], [6], [11], AND THIS WORK

Ref.	Method	Frequency	Radius of winding	L	Q	Output power	Power per m^2	Efficiency
[4]	Parameters design	500 kHz	70.7 mm	3.75 μH	71.84	109.42 W	7 kW/m^2	75%
[6]	Litz structure	85 kHz	190 mm	39.51 μH	167.5	3300 W	29 kW/m^2	88%
[11] (@MC-WPT)	Self-resonant	3 MHz	105 mm	39.3 μH	322	252.7 W	7.3 kW/m^2	90.5%
This work	Split impedance tuning	300 kHz	76 mm	19.7 μH	113.9	527 W	29 kW/m^2	90%

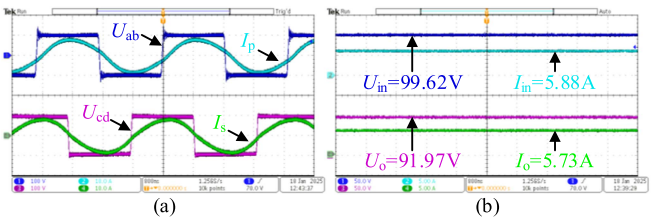

Fig. 8. Experimental waveforms with rated output. (a) Output of the inverter and input of the rectifier. (b) Input of the inverter and output of the rectifier.

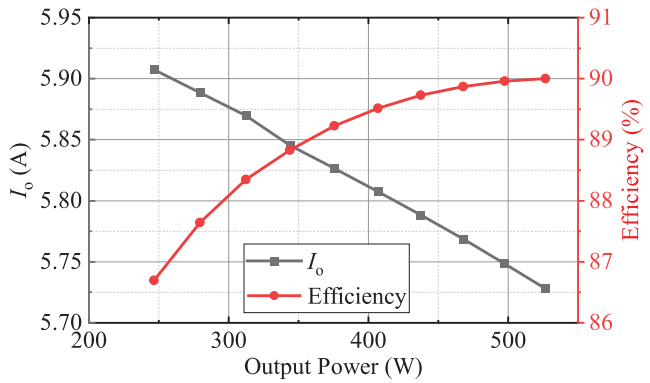

Fig. 9. Curves of output current and efficiency versus output power.

The operation frequency of the system is 300 kHz. MOSFETs S_1–S_4 adopts C2M0080120D. The models of diodes D_1–D_4 are STPS60SM200CW. Both the transmitter and receiver are PCB windings, which together form a coupler, with a vertical distance of 50 mm. The electrical parameters of the WPT system are summarized in Table II.

Fig. 8 shows the voltage and current waveforms measured during the experiment with rated output (527 W).

As shown in Fig. 9, at an input voltage of 100 V, the output current (I_o) decreases as the output power increases. The maximum current of 5.91 A occurs at 246 W, while the minimum current of 5.73 A is observed at 527 W. Overall, the output current fluctuates by 3%. The efficiency of the WPT system (from dc to dc) reaches a maximum of 90% at an output power of 527 W, the efficiency is at its minimum of 86.7% at an output power of 246 W.

Based on the experimental data and the datasheets of the MOSFET and diode, the loss distribution can be derived from (22) to (24). Fig. 10 illustrates the loss distribution and measured efficiency of the system under rated output power (527 W), with the coupler loss accounted for as 47.6% (27.1 W).

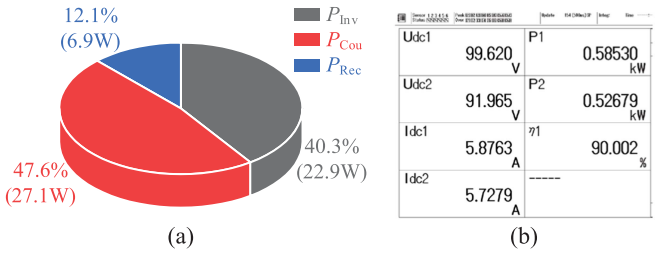

Fig. 10. Loss distribution and measured efficiency with rated output power (527 W). (a) Loss distribution. (b) Measured efficiency.

Table III tabulates the comparison between this work and others' work in terms of frequency, size, inductance L, quality factors Q, output power, power per m^2, and system efficiency. By adopting the proposed method, the system achieves 90% efficiency and a power density of 29 kW/m^2 on the experimental platform at a frequency of 300 kHz.

Compared with parameter design, better resistance optimization can be achieved without an exact PCB winding model and extensive simulation optimization. Compared to the Litz structure, the Litz configuration is more complex in terms of modeling and demands substantial computational resources for simulation validation. In addition, the Litz structure involves the alternating winding of multiple strands of wire, which poses challenges in achieving optimal resistance performance in compact designs. Compared to self-resonant systems, it offers a lower operating frequency and higher power density.

V. CONCLUSION

This letter presents a split impedance tuning method for optimizing the resistance of PCB windings. By using capacitors to compensate for the impedance of each wire, the optimal currents distribution is achieved, thereby reducing the resistance of the winding and enhancing the overall efficiency of the system. Compared with the previous methods for optimizing the resistance of PCB windings, the proposed method is simple in design, only reducing the equivalent resistance of the PCB windings through capacitors, and does not rely on the parameters of the PCB winding itself, without restrictions such as frequency and PCB winding size. Through experimental validation, the resistance of the winding, originally 0.904 Ω, can be reduced to 0.326 Ω after applying the split impedance tuning method. Finally, the WPT system experimental platform was built, achieving a maximum system efficiency of 90% at an output of 527 W.

REFERENCES

[1] S. Jeong et al., "Smartwatch strap wireless power transfer system with flexible PCB coil and shielding material," *IEEE Trans. Ind. Electron.*, vol. 66, no. 5, pp. 4054–4064, May 2019.

[2] C. Cai et al., "Multi-state voltage balancing of UAV's cell string: A reconfigurable WPT based multiport hybrid charging approach," *IEEE Trans. Ind. Electron.*, vol. 72, no. 1, pp. 266–277, Jan. 2025.

[3] K. Chen and Z. Zhao, "Analysis of the double-layer printed spiral coil for wireless power transfer," *IEEE J. Emerg. Sel. Topics Power Electron.*, vol. 1, no. 2, pp. 114–121, Jun. 2013.

[4] X. Du and D. Dujic, "Modeling and design optimization of loosely coupled PCB spiral coils in inductive power transfer systems," *IEEE Trans. Power Electron.*, vol. 38, no. 11, pp. 13430–13442, Nov. 2023.

[5] I. Lope, C. Carretero, J. Acero, R. Alonso, and J. M. Burdio, "Frequency-dependent resistance of planar coils in printed circuit board with litz structure," *IEEE Trans. Magn.*, vol. 50, no. 12, Dec. 2014, Art. no. 8402409.

[6] A. Narvaez, C. Carretero, I. Lope, and J. Acero, "Printed circuit board coils of multitrack litz structure for 3.3-kW inductive power transfer system," *IEEE Trans. Transp. Electrific.*, vol. 9, no. 3, pp. 3947–3957, Sep. 2023.

[7] Z. Wang et al., "Equally split PCB inductor (ESPI) design for high energy density and low near-field radiation," *IEEE Trans. Power Electron.*, vol. 39, no. 5, pp. 4963–4968, May 2024.

[8] K. Li, J. Wu, A. C. Yucel, and S. -Y. R. Hui, "New printed-circuit-board resonators with high quality factor and transmission efficiency for megahertz wireless power transfer applications," *IEEE Trans. Power Electron.*, vol. 38, no. 10, pp. 13207–13218, Oct. 2023.

[9] Y. Fang, J. Qu, B. M. H. Pong, C. K. Lee, and R. S. Y. Hui, "Quasi-static modeling and optimization of two-layer PCB resonators in wireless power transfer systems for 110-kV power grid online monitoring equipment," *IEEE Trans. Ind. Electron.*, vol. 69, no. 2, pp. 1400–1410, Feb. 2022.

[10] R. Qin, J. Li, and D. Costinett, "A 6.6-kW high-frequency wireless power transfer system for electric vehicle charging using multilayer nonuniform self-resonant coil at MHz," *IEEE Trans. Ind. Electron.*, vol. 37, no. 4, pp. 4842–4856, Apr. 2022.

[11] Y. Wang, K. Wang, K. Li, Y. Yang, and S. Y. R. Hui, "Multi-MHz inductive and capacitive power transfer systems with PCB-based self-resonators," *IEEE Trans. Power Electron.*, vol. 39, no. 10, pp. 14077–14090, Oct. 2024.

[12] Y. Cho et al., "Thin PCB-type metamaterials for improved efficiency and reduced EMF leakage in wireless power transfer systems," *IEEE Trans. Microw. Theory Techn.*, vol. 64, no. 2, pp. 353–364, Feb. 2016.

[13] Y. Li et al., "Extension of ZVS region of series–series WPT systems by an auxiliary variable inductor for improving efficiency," *IEEE Trans. Power Electron.*, vol. 36, no. 7, pp. 7513–7525, Jul. 2021.